Dendritic lipopeptide liposomes decorated with dual-targeted protein

Sensen Zhou[a], Cheng Li[a], Yang Yuan[a], Lei Jiang[a,b], Weizhi Chen*[a], Xiqun Jiang*[a]*

[a]Department of Polymer Science & Engineering, College of Chemistry & Chemical Engineering, and Jiangsu Key Laboratory for Nanotechnology, Nanjing University, Nanjing, 210023, P.R. China.

[b]State Key Laboratory of Natural Medicines, Department of Pharmaceutics, China Pharmaceutical University, 24 Tongjiaxiang, Nanjing 210009, China.

* To whom correspondence should be addressed: jiangx@nju.edu.cn; chenwz@nju.edu.cn; jianglei0453@163.com.

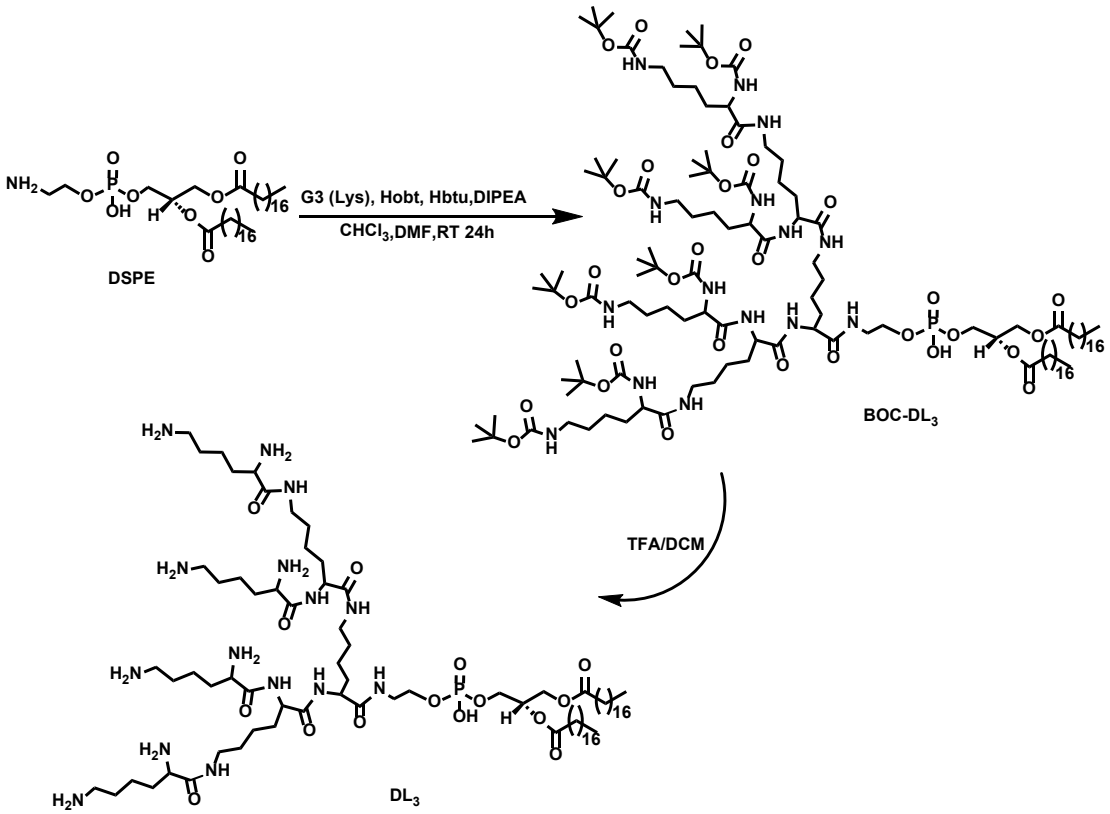

Fig. S1 Synthesis procedure of DL_3.

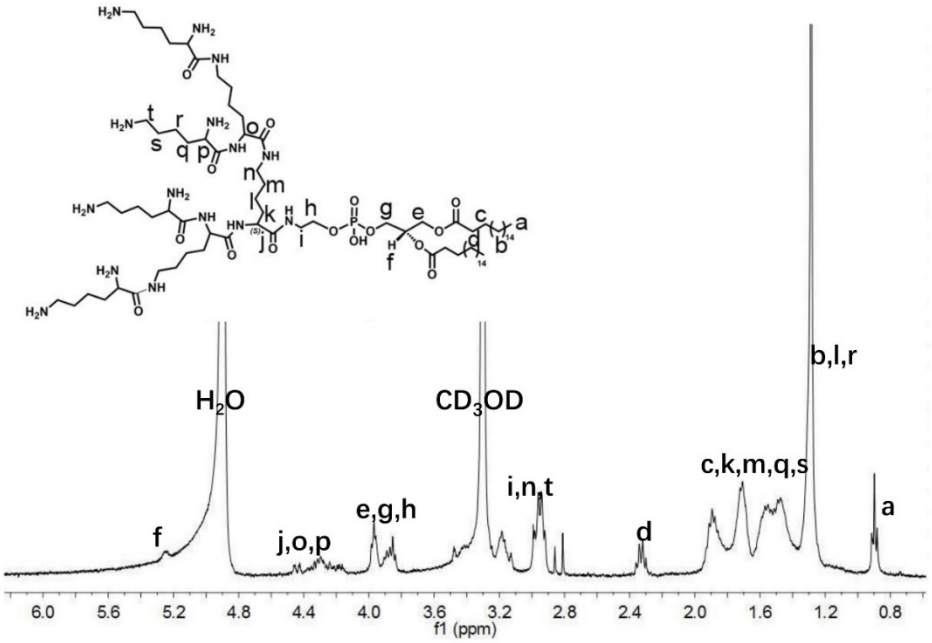

Fig. S2 ^{1}H-NMR spectrum of DL3 in CH_3DO.

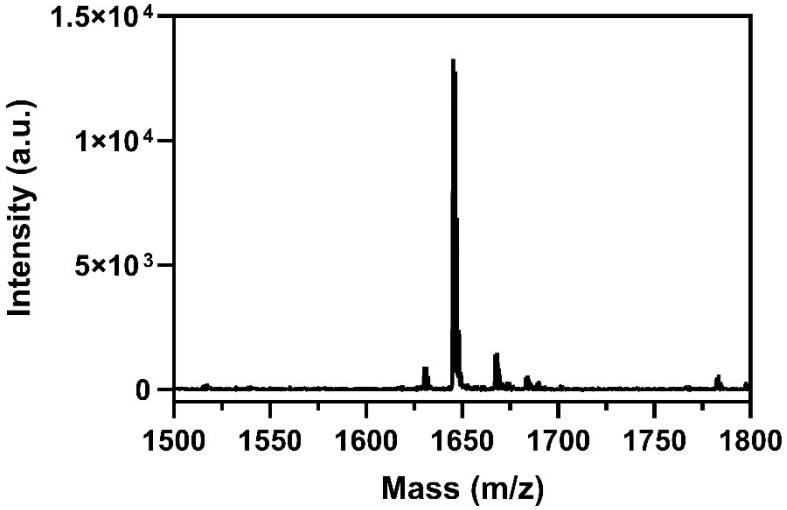

Fig. S3 MALDI-TOF MS of DL_3.

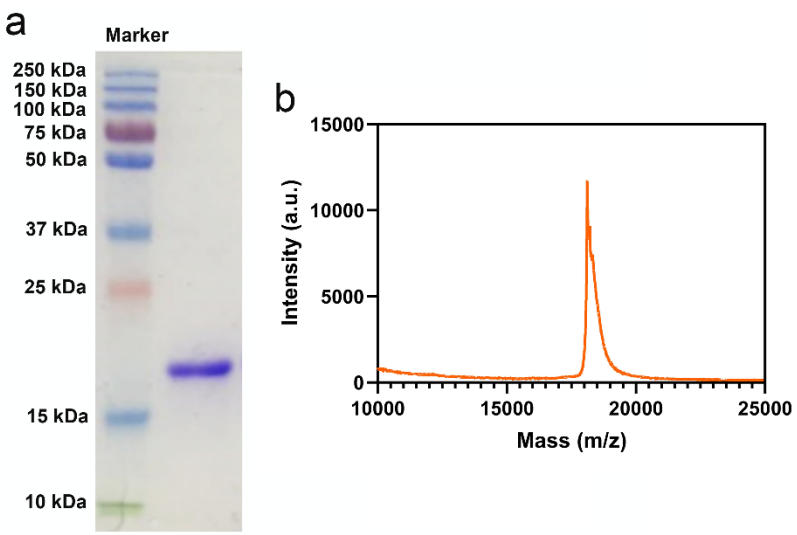

Fig. S4 (a) The SDS-PAGE of recombinant protein RP-ER; (b) MALDI-TOF MS of RP-ER in 50% acetonitrile aqueous solution with 0.1% trifluoroacetic acid with sinapic acid as the matrix.

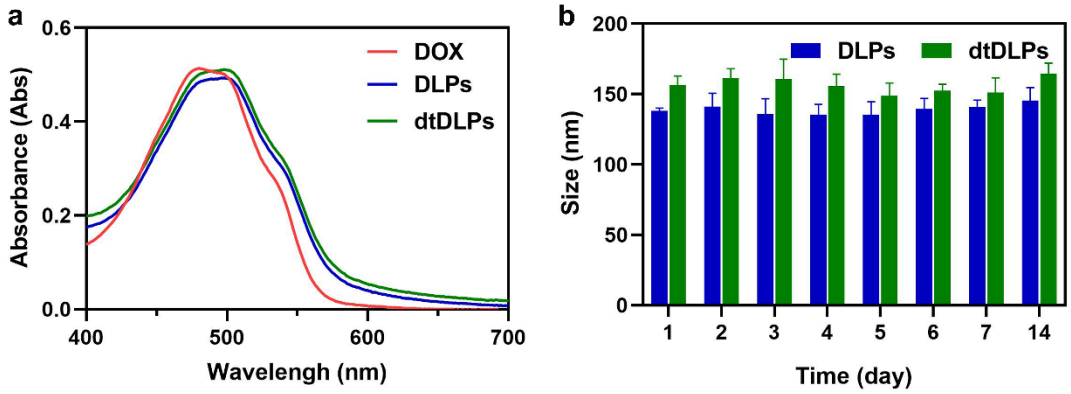

Fig. S5 (a) UV-Vis absorption spectra of DOX, DLPs and dtDLPs in 10 mM PBS. (b) the stability of DLPs and dtDLPs measured by DLS. Data are presented as mean ± s.d., n = 3.

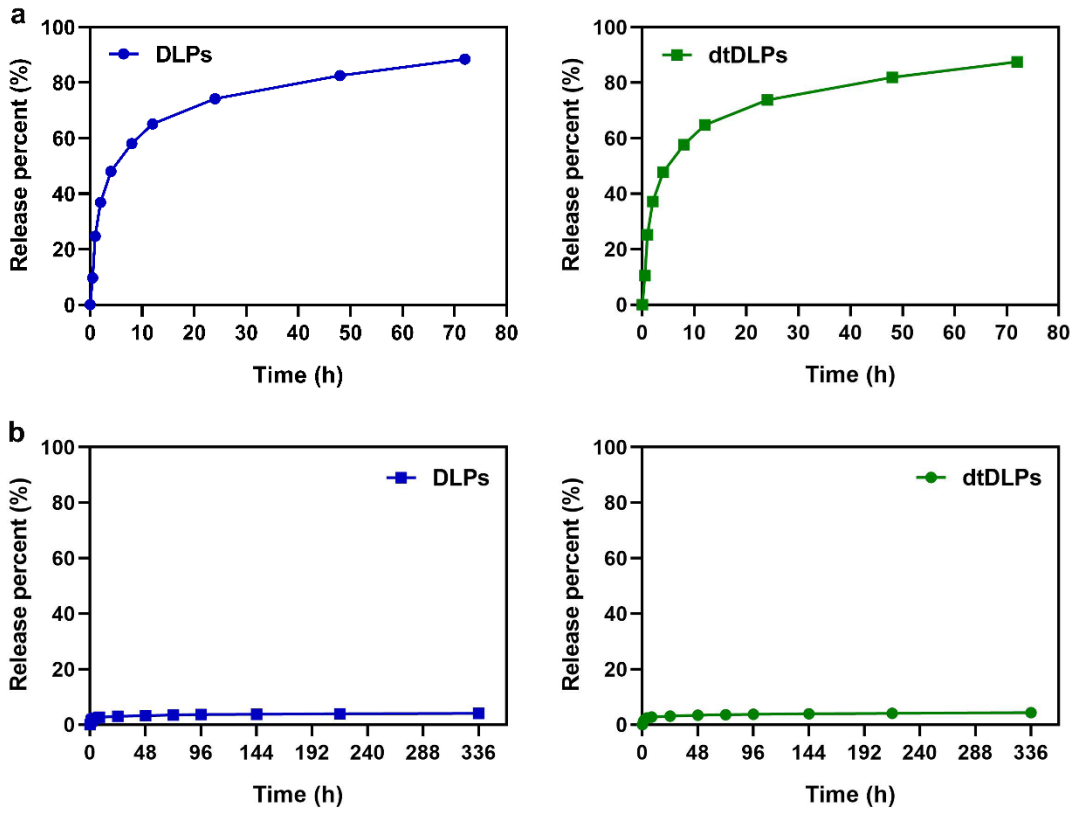

Fig. S6 (a) In vitro release profiles of DOX from DLPs and dtDLPs in 0.01 M PBS with 0.5% tween 20 at pH 7.4 at 37 °C with 200 rpm. (b) In vitro release profiles of DOX from DLPs and dtDLPs in 0.01 M PBS at pH 7.4 at 4 °C with 200 rpm. Data are presented as mean ± s.d., n = 3.

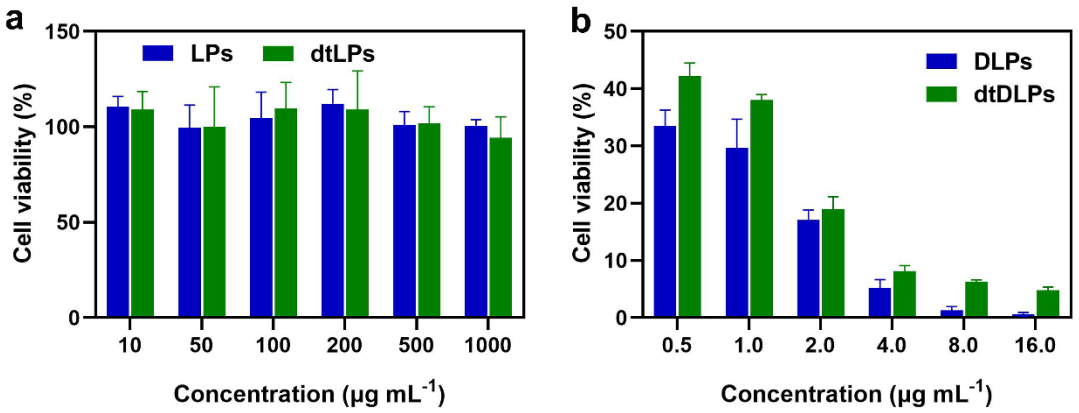

Fig. S7 Cytotoxicity of LPs and tLPs (a) and DLPs and dtDLPs (b) in RAW264.7 cells evaluated by MTT assay. Data are presented as mean ± s.d., n = 3.

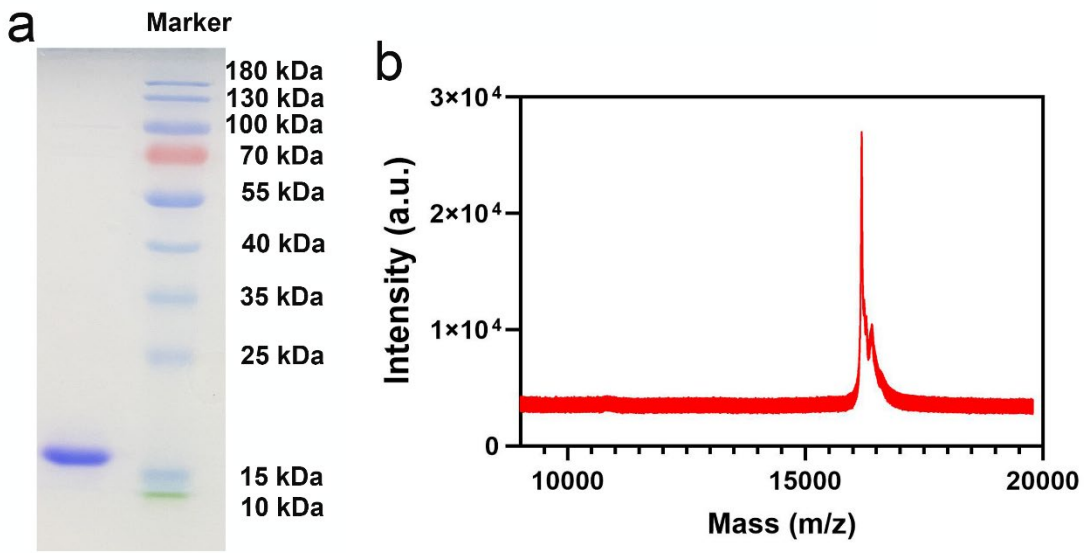

Fig. S8 (a) The SDS-PAGE of recombinant protein RP-E; (b) MALDI-TOF MS of RP-E in 50% acetonitrile aqueous solution with 0.1% trifluoroacetic acid with sinapic acid as the matrix.

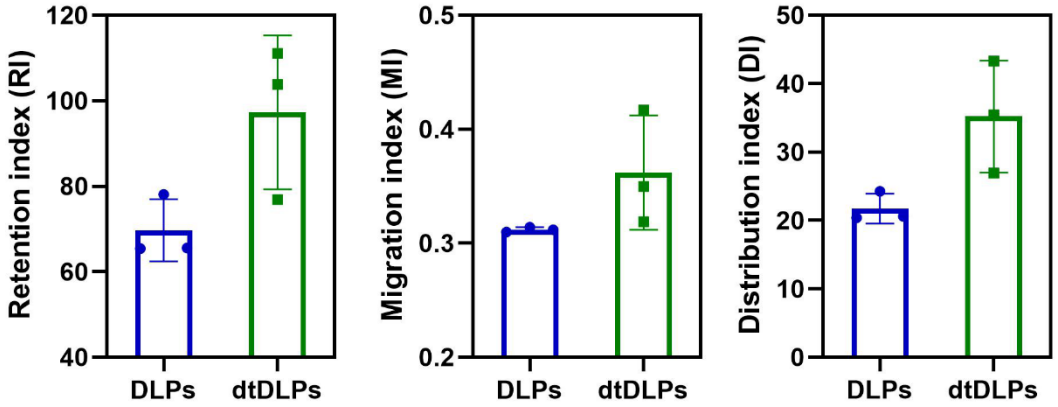

Fig. S9 Drug distribution of DLPs and dtDLPs evaluated by DI, MI and RI in HeLa MCs. Data are presented as mean ± s.d., n = 3.

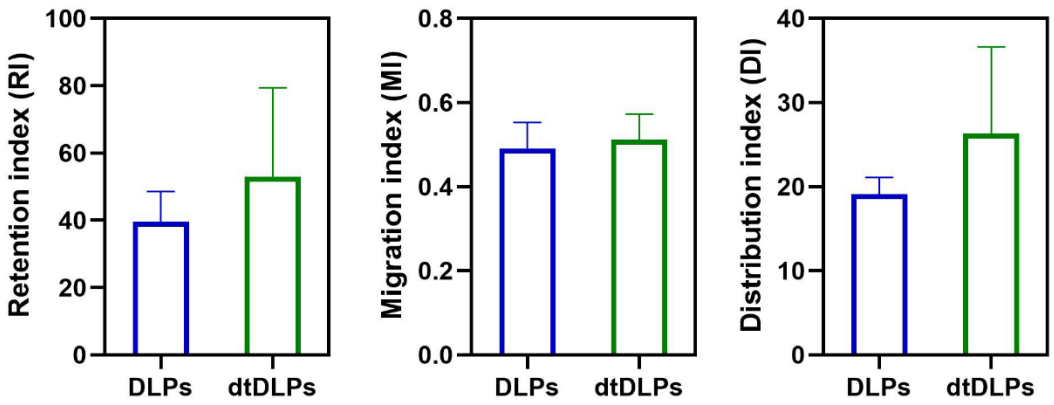

Fig. S10 Drug distribution of DLPs and dtDLPs evaluated by DI, MI and RI in 4T1 MCs. Data are presented as mean ± s.d., n = 2.

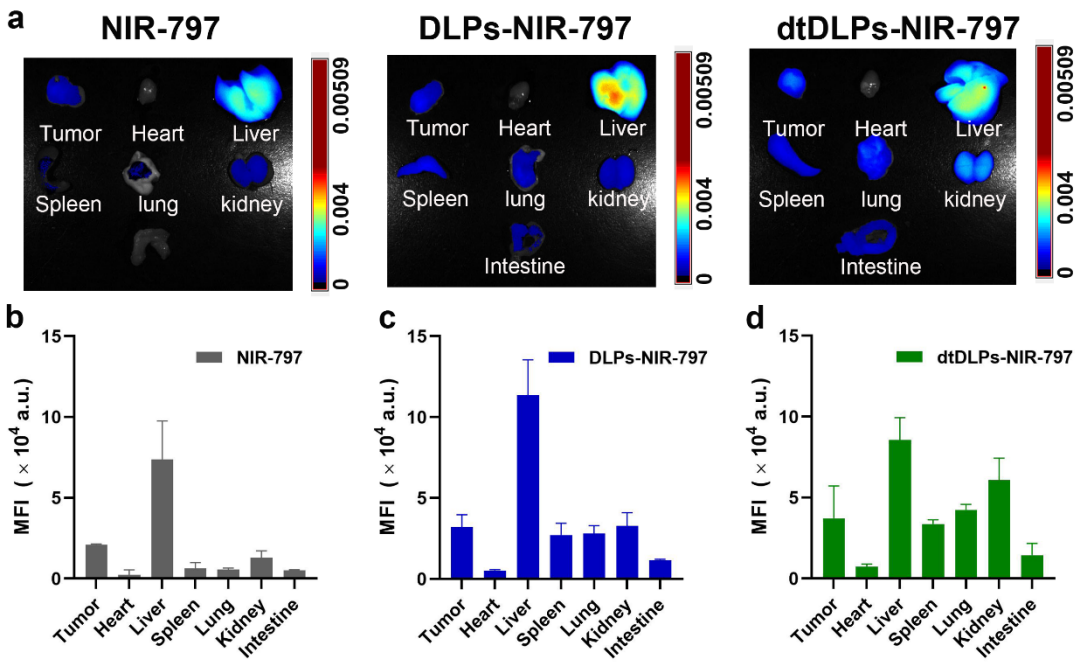

Fig. S11 (a) The NIRF images of the organs collected from the mice injected with free NIR-797, NIR-797 labeled DLPs and dtDLPs for 72 h. The MFIs in each organ for NIR-797 (b), DLPs-NIR-797 (c) and dtDLPs-NIR-797 (d) were quantified. Data are presented as mean ± s.d., n = 2 for NIR-797 group, 3 for DLPs and dtDLPs group.

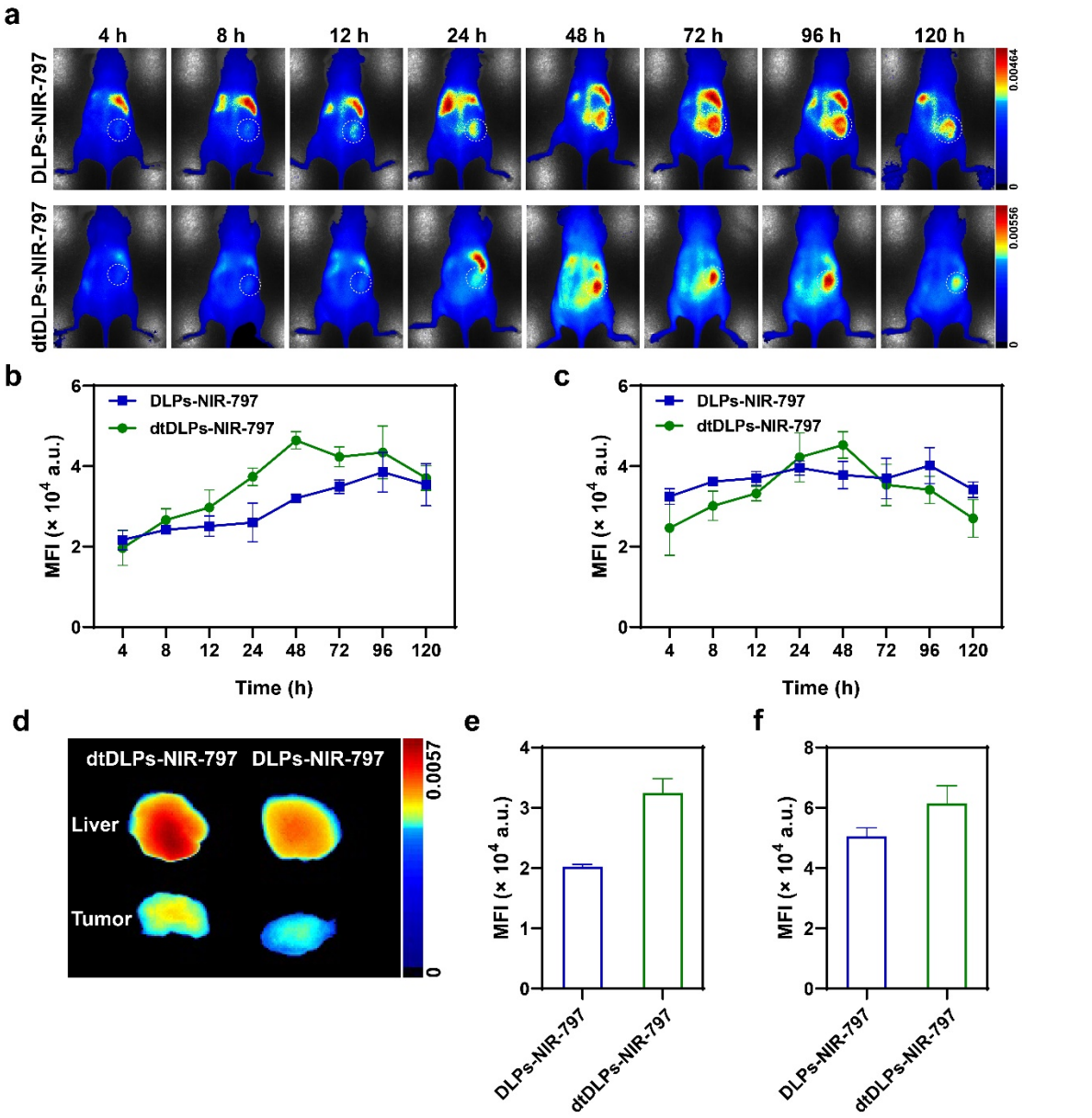

Fig. S12 (a) The in vivo NIRF images of HeLa tumor-bearing mice following intravenous injection of DLPs-NIR-797 and dtDLPs-NIR-797 at different time points. The tumors were surrounded with dotted lines. The MFIs in tumors (b) and livers (c) for different agents at different times were measured from the NIRF images. (d) At the end of experiment, the livers and tumors were taken out for NIRF imaging. The MFIs for livers (e) and tumors (f) collected from different group were measured. Data are presented as mean ± s.d., n = 2 for each group.

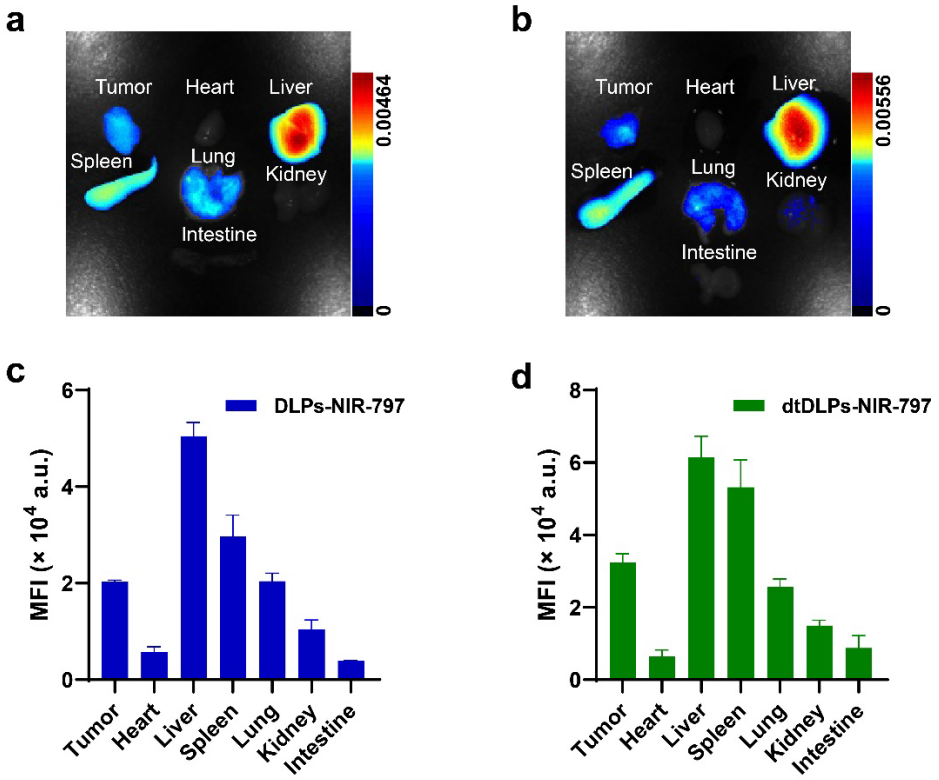

Fig. S13 The NIRF images of the organs collected from the mice injected with NIR-797 labeled DLPs (a) and dtDLPs (b) for 120 h. The MFIs in each organ for DLPs-NIR-797 (c) and dtDLPs-NIR-797 (d) were quantified. Data are presented as mean ± s.d., n = 2 for each group.

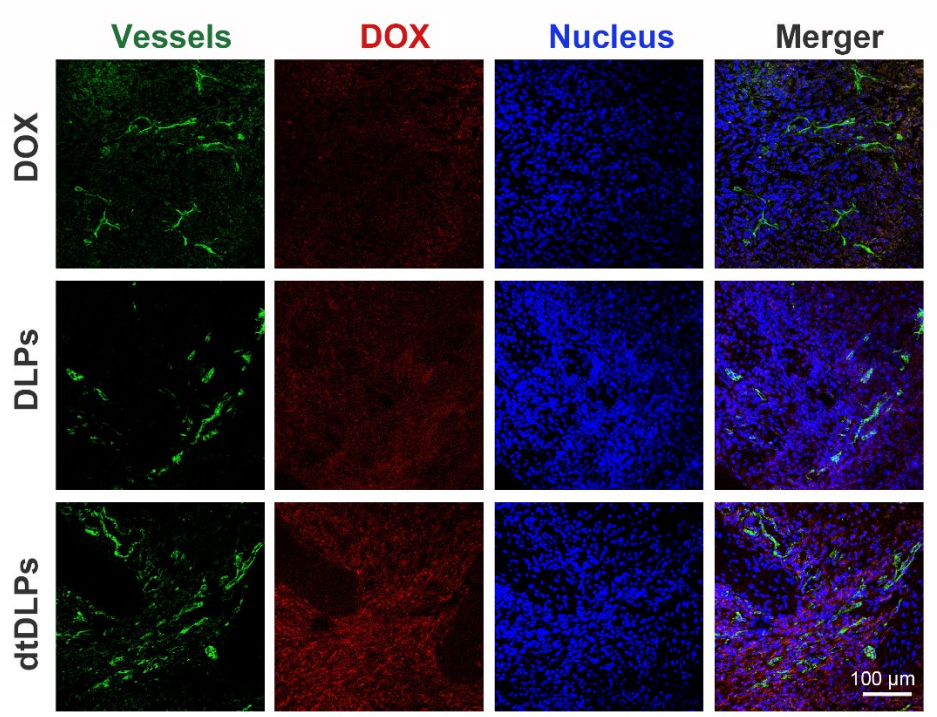

Fig. S14 CLSM images of the penetration of free DOX, DLPs and dtDLPs in 4T1 tumors at 24 h post-injection. The CD31 antibody were used to stained the blood vessels (green). The nucleuses were stained as blue by DAPI.

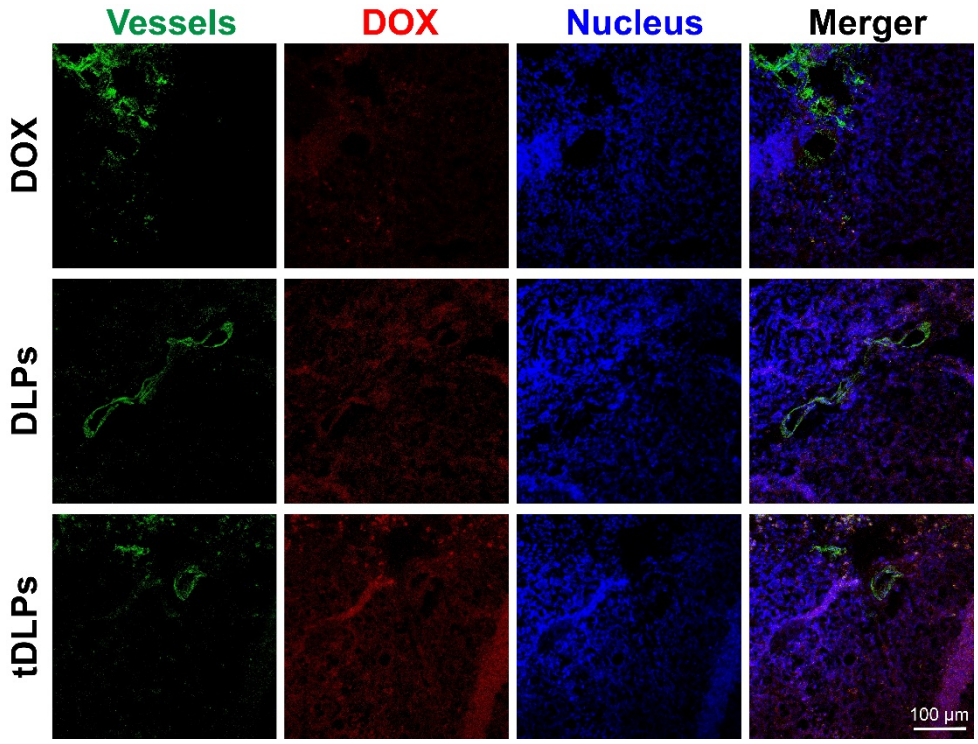

Fig. S15 CLSM images of the penetration of free DOX, DLPs and dtDLPs in HeLa tumors at 24 h post-injection. The CD31 antibody were used to stained the blood vessels (green). The nucleuses were stained as blue by DAPI.

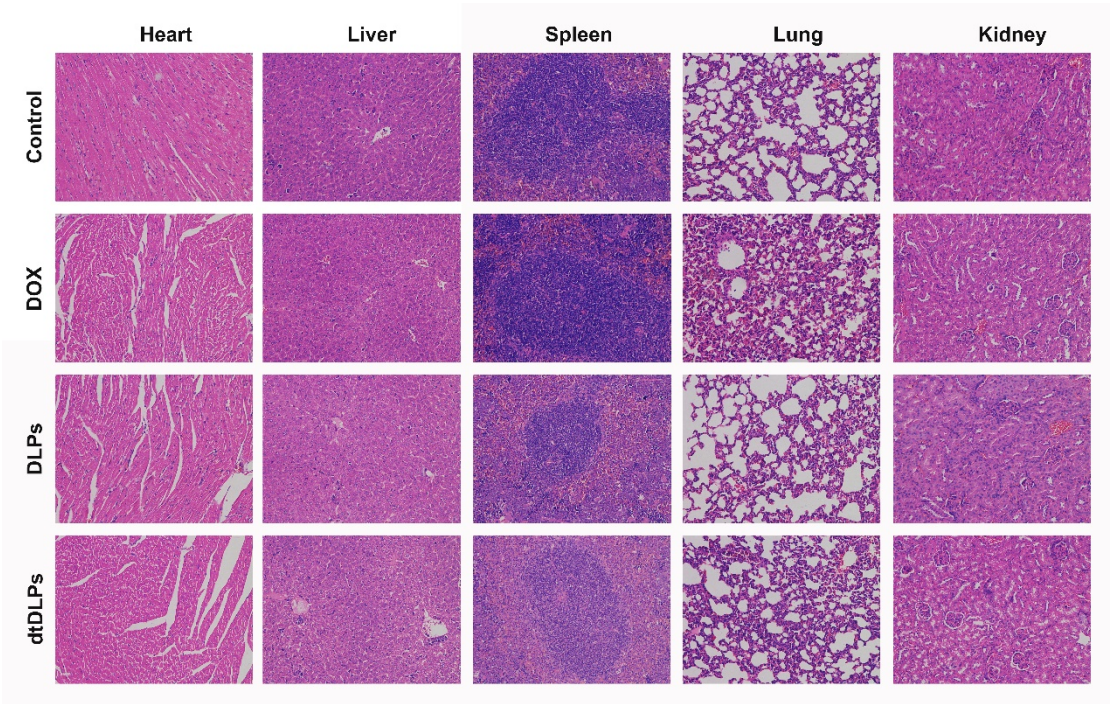

Fig. S16 The H&E staining of the major organs of different groups at the end of anticancer efficacy experiment in 4T1 tumor-bearing mice.

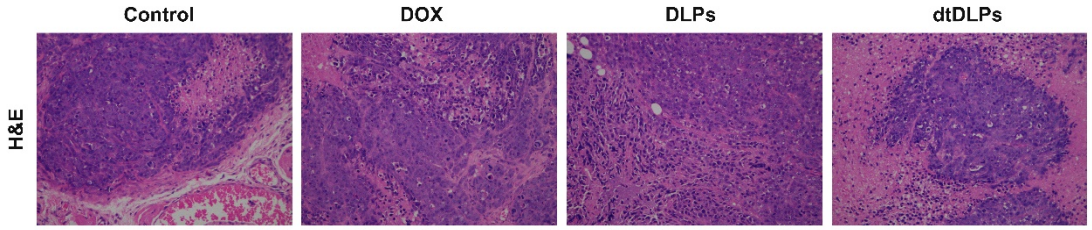

Fig. S17 The H&E staining of the HeLa tumors of different groups at the end of anticancer efficacy experiment.

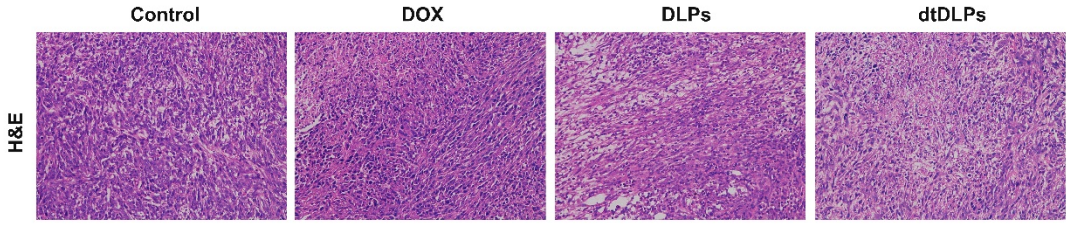

Fig. S18 The H&E staining of the 4T1 tumors of different groups at the end of anticancer efficacy experiment.